Available online at www.sciencedirect.com
SCIENCE DIRECT®
Journal of Sound and Vibration 284 (2005) 635–650
JOURNAL OF SOUND AND VIBRATION
www.elsevier.com/locate/jsvi

Electro-dynamics, micro-actuation and design of arc stators in an ultrasonic curvilinear motor

P. Smithmaitrie[a], H.S. Tzou[b,*]

[a]*Department of Mechanical Engineering, Faculty of Engineering, Prince of Songkla University, Songkla 90112, Thailand*
[b]*Department of Mechanical Engineering, StrucTronics Laboratory, University of Kentucky, Lexington, KY 40506-0503, USA*

Received 15 October 2003; accepted 29 June 2004
Available online 18 November 2004

Abstract

Driving mechanisms basically deliver two fundamental motions, i.e., linear and curvilinear motions. A piezoelectric laminated circular arc can serve as a curvilinear arc stator to deliver curvilinear motion on a spherical surface. This study is to evaluate ultrasonic vibration characteristics and microscopic membrane/bending actuation forces of piezoelectric actuators laminated on a curvilinear circular arc. Mathematical model and governing equations of circular arcs bonded with piezoelectric actuator patches are derived, followed by analysis of actuator control forces and moments and micro-control actions in the modal domain. A study of vibration characteristics is conducted to design an optimal actuator configuration, e.g., size and location. Then, distributed control forces and micro-control actions of the curvilinear arc stator are analyzed with respect to key design parameters (i.e., arc radius, arc thickness and actuator thickness). Study of stator vibration behavior clearly suggests an optimal actuator size and location to efficiently excite the desirable ultrasonic natural mode dominated by the micro-bending control action.

1. Introduction

As the mechatronics and structronics areas keep expanding, scientists have been continuously developing and testing piezoelectric or electrostrictive ultrasonic motors and drivers [1–3]. The

*Corresponding author. Tel.: +1 606 257 6336; fax: +1 606 257 3304.
E-mail address: hstzou@engr.uky.edu (H.S. Tzou).

0022-460X/$ - see front matter © 2004 Elsevier Ltd. All rights reserved.
doi:10.1016/j.jsv.2004.06.039

principle of ultrasonic motors is to utilize ultrasonic oscillations (or waves) generated by piezoelectric or electrostrictive actuators to create forces (or torques) driving the rotor by friction on contact surfaces. Most ultrasonic vibration actuators are based on piezoelectric materials bonded on motor structures designed for either linear or rotary motions. This study is to investigate electro-dynamics and micro-actuation characteristics of a curvilinear arc stator driving a curvilinear arc motor.

Piezoelectric structures and components have been being applied to many engineering applications, such as vibration control [4–6], sensors/actuators [7,8], ultrasonic motors [1,2], etc. Micro-control forces and actuations of various piezoelectric shells, such as conical shells [9], paraboloidal shells [10] and spherical shells [11], have been recently investigated. Dynamic characteristic and vibration control of piezoelectric circular arc structures were also studied [12–15]. This study is to evaluate microscopic actuation forces of piezoelectric actuators laminated on a curvilinear circular arc specifically applied to curvilinear arc drivers and motors.

In this study, vibration characteristics and micro-control actions of the piezoelectric circular arc stator are investigated. Mathematical modeling and governing equations of a circular arc bonded with piezoelectric actuator patches are derived first, followed by analysis of actuator control forces and moments and micro-control actions in the modal domain. Study of vibration characteristics is conducted to select actuator configuration and layout. Then, distributed control forces and contributing micro-control actions are analyzed with respect to key stator design parameters (e.g., arc radius, arc thickness, actuator thickness).

2. Dynamics of a circular arc stator

A curvilinear arc stator driving a curvilinear arc motor is illustrated in Fig. 1; its dynamic characteristics and vibration behavior are analyzed in this section. The circular arc stator drives and guides a rotor along the circular arc to any prescribed angular position on the arc surface. Fig. 1 also illustrates the arc coordinate system defined as $\alpha_1 = \phi$, $\alpha_2 = y$ and $\alpha_3 = 3$. The Lamé parameters corresponded to the arc coordinates are $A_1 = R$ and $A_2 = 1$ and the radii of curvature

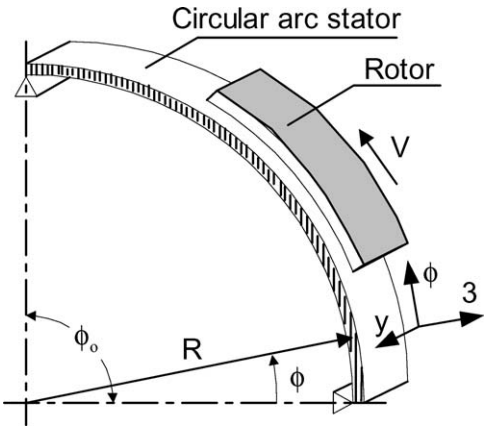

Fig. 1. Schematic diagram of the curvilinear arc stator/motor.

are $R_1 = R$ and $R_2 = \infty$. Dynamics and modal characteristics of the arc stator is investigated in this section.

A circular arc is assumed slender, i.e., the ratio of thickness to length is very small. Thus, the thin shell theory can be applied to define the system equations. Assumed that there are no deflections in the y-direction (depth direction) and changes relative to the y-direction can be neglected. Hence there are two equations of motion, respectively, in the ϕ- and transverse-directions describing the arc dynamics; Fig. 2.

Substituting the Lamé parameters and radii of curvature into the system equations of a generic double-curvature thin shell [4] and simplifying yields the equations of motion of the arc stator respectively in the u_ϕ- and u_3-directions:

$$-\frac{\partial N_{\phi\phi}}{\partial \phi} - Q_{\phi 3} + R\rho h \frac{\partial^2 u_\phi}{\partial t^2} = Rq_\phi, \tag{1}$$

$$-\frac{\partial Q_{\phi 3}}{\partial \phi} + N_{\phi\phi} + R\rho h \frac{\partial^2 u_3}{\partial t^2} = Rq_3, \tag{2}$$

$$Q_{\phi 3} = \frac{1}{R}\frac{\partial M_{\phi\phi}}{\partial \phi}, \tag{3}$$

where $N_{\phi\phi}$ is the membrane force; $M_{\phi\phi}$ is the bending moment; $Q_{\phi 3}$ denotes the traverse shear stress resultant; R is the radius; q_i is the external excitation; ρ is the mass density; h is the shell thickness, and u_i is the displacement in the i-direction. Note that q_i can also be discrete or distributed control forces. Membrane force $N_{\phi\phi}$ and bending moment $M_{\phi\phi}$ are functions of membrane strains s^o_{ij} and bending strains k_{ij} defined as

$$N_{\phi\phi} = K(s^\circ_{\phi\phi} + \mu s^\circ_{yy}), \quad M_{\phi\phi} = D(k_{\phi\phi} + \mu k_{yy}), \tag{4,5}$$

where $K = (Yh)/(1-\mu^2)$ is the membrane stiffness; $D = (Yh^3)/[12(1-\mu^2)]$ is the bending stiffness; Y is Young's modulus; and μ is Poisson's ratio. The strain–displacement relations of the thin arc stator are

$$s^\circ_{yy} = 0, \quad s^\circ_{\phi\phi} = \frac{1}{R}\left(\frac{\partial u_\phi}{\partial \phi} + \frac{u_3}{R}\right), \tag{6,7}$$

$$k_{yy} = 0, \quad k_{\phi\phi} = \frac{1}{R}\frac{\partial \beta_\phi}{\partial \phi} \tag{8,9}$$

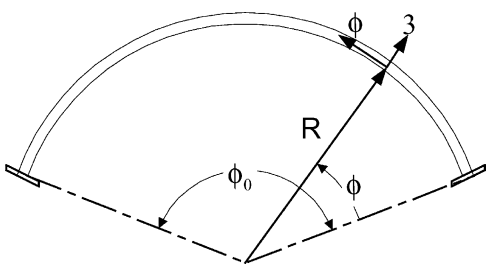

Fig. 2. Coordinate system of a circular arc.

and the rotation angle $\beta_\phi = 1/R(u_\phi - (\partial u_3/\partial\phi))$. Substituting Eqs. (3)–(9) into Eqs. (1) and (2) yields the equations of motion in the ϕ- and transverse-directions, respectively, as

$$\frac{D}{R^4}\left(\frac{\partial^2 u_\phi}{\partial\phi^2} - \frac{\partial^3 u_3}{\partial\phi^3}\right) + \frac{K}{R^2}\left(\frac{\partial^2 u_\phi}{\partial\phi^2} + \frac{\partial u_3}{\partial\phi}\right) + q_\phi = \rho h \frac{\partial^2 u_\phi}{\partial t^2}, \tag{10}$$

$$\frac{D}{R^4}\left(\frac{\partial^3 u_\phi}{\partial\phi^3} - \frac{\partial^4 u_3}{\partial\phi^4}\right) - \frac{K}{R^2}\left(\frac{\partial u_\phi}{\partial\phi} + u_3\right) + q_3 = \rho h \frac{\partial^2 u_3}{\partial t^2}. \tag{11}$$

Even and odd transverse flexural mode shapes U_{ij} and natural frequencies f_k of a circular arc with simply supported boundary condition are, respectively, defined as follows [17,18], for $k = 2, 4, 6, \ldots$:

$$f_k = \frac{k^2\pi^2}{2\pi(R\phi_0)^2}\left[\frac{\left\{1 - \left(\frac{\phi_0}{k\pi}\right)^2\right\}^2}{1 + 3\left(\frac{\phi_0}{k\pi}\right)^2}\right]^{1/2}\sqrt{\frac{YI}{m}}, \tag{12}$$

$$U_{\phi k} = \frac{\phi_0}{k\pi}\left[1 - \cos\left(\frac{k\pi\phi}{\phi_0}\right)\right], \quad U_{3k} = -\sin\left(\frac{k\pi\phi}{\phi_0}\right), \tag{13,14}$$

and for $k = 3, 5, 7, \ldots$:

$$f_k = \frac{k^2\pi^2}{2\pi(R\phi_0)^2}\left[\frac{\left\{1 - \left(\frac{\phi_0}{k\pi}\right)^2\right\}^2}{1 + \frac{1}{k^2} + 2\left(\frac{\phi_0}{k\pi}\right)^2}\right]^{1/2}\sqrt{\frac{YI}{m}}, \tag{15}$$

$$U_{\phi k} = -\frac{\phi_0}{k\pi}\left[\cos\left(\frac{k\pi\phi}{\phi_0}\right) - \frac{1}{\pi^3}\cos\left(\frac{\pi\phi}{\phi_0}\right)\right], \quad U_{3k} = -\sin\left(\frac{k\pi\phi}{\phi_0}\right) + \frac{1}{k}\sin\left(\frac{\pi\phi}{\phi_0}\right), \tag{16,17}$$

where k is the mode number; f_k is the natural frequency in Hz; Y is the modulus of elasticity; I is the area moments of inertia; m is the mass per unit length; $U_{\phi k}$, U_{3k} are the kth flexural mode shapes corresponding to ϕ- and transverse-direction; ϕ is the angular position of the arc; ϕ_0 is opening angle of the arc. The main objective of the study is to evaluate the actuator induced spatial actuation characteristics in order to select the optimal segmentation design for the curvilinear arc stator. Although the physical properties of piezoelectric patches are neglected in the modal analysis, they are included in the actuation force/moment components. Further studies of stator/motor characteristics of the curvilinear motor system indicate that (1) the influence of polymeric patches can be neglected and that of ceramic actuators cannot be neglected and (2) the analytical and finite element solutions of a ceramic stator/motor system compare very well [16].

3. Micro-control actions of a circular arc stator

A piezoelectric patch bounded on the circular arc stator introduces control forces and moments resulting in curvilinear driving actions. The effect of control force $N^c_{\phi\phi}$ and moment $M^c_{\phi\phi}$ induced by the actuator patch can be added to the dynamic equations of the circular arc (1) and (2), and written as

$$\frac{\partial(N_{\phi\phi} - N^c_{\phi\phi})}{\partial\phi} + Q_{\phi 3} + Rq_\phi = R\rho h\frac{\partial^2 u_\phi}{\partial t^2}, \tag{18}$$

$$\frac{\partial Q_{\phi 3}}{\partial\phi} - (N_{\phi\phi} - N^c_{\phi\phi}) + Rq_3 = R\rho h\frac{\partial^2 u_3}{\partial t^2}, \tag{19}$$

and

$$Q_{\phi 3} = \frac{1}{R}\frac{\partial(M_{\phi\phi} - M^c_{\phi\phi})}{\partial\phi}. \tag{20}$$

The forced response of the arc can be determined by the modal participation method. It is assumed that the excitation force is independent of the shell motion and that the amount of participation of each mode in the total dynamic response is defined by the modal participation factor [19]. Thus, the total response of the arc, i.e., $u_i(\phi, t)$, can be written as

$$u_i(\phi, t) = \sum_{k=2}^{\infty} \eta_k(t) U_{ik}(\phi), \tag{21}$$

where $i = \phi, 3$; $\eta_k(t)$ is the modal participation factor and $U_{ik}(\phi)$ is the mode shape function in the i-direction. Using Eq. (21), integrating over the surface, and imposing modal orthogonality, one can derive the kth modal equation of the circular arc as

$$\ddot{\eta}_k + 2\zeta_k\omega_k\dot{\eta}_k + \omega_k^2\eta_k = \hat{F}^m_k(t) + \hat{F}^c_k(t) \equiv \hat{F}_k(t), \tag{22}$$

where the modal damping ratio $\zeta_k = c/(2\rho h\omega_k)$ and c is the damping factor usually experimentally estimated; ω_k is the kth mode natural frequency; $\hat{F}^m_k(t)$ is the mechanical excitation; $\hat{F}^c_k(t)$ is the electrical control excitation; $\hat{F}_k(t)$ is the total modal control force. In this case, it is assumed that the mechanical excitation is neglected, thus the excitation force is only the electrical control excitation. Then the modal control force $\hat{F}_k(t)$ becomes

$$\hat{F}_k(t) = \frac{1}{\rho h N_k}\int_y\int_\phi \left\{\sum_i L^c_i(\phi^a) U_{ik}\right\} A_1 A_2\,\mathrm{d}\phi\,\mathrm{d}y, \quad i = \phi, 3, \tag{23}$$

where $N_k = \int_y\int_\phi\{\sum_i U^2_{ik}\}A_1A_2\,\mathrm{d}\phi\,\mathrm{d}y$; $L^c_i(\phi^a)$ is a Love's operator derived from the converse piezoelectric effect and it is assumed that only a transverse voltage ϕ^a is considered [4]. Also, note

that $L_i^c(\phi^a)$ is a function of time and spatial coordinate. Thus,

$$L_\phi^c(\phi^a) = -\frac{1}{R}\left(\frac{\partial N_{\phi\phi}^c}{\partial\phi} + \frac{1}{R}\frac{\partial M_{\phi\phi}^c}{\partial\phi}\right), \tag{24}$$

$$L_3^c(\phi^a) = -\frac{1}{R}\left(\frac{1}{R}\frac{\partial^2 M_{\phi\phi}^c}{\partial\phi^2} - N_{\phi\phi}^c\right). \tag{25}$$

3.1. Control forces and moments

The circular arc stator is bonded with a piezoelectric driver patch defined from ϕ_1 to ϕ_2 in the angular position and has the same width as the arc stator b as illustrated in Fig. 3. The patch serves as the primary driver producing forward/backward waves on the circular arc stator. It is assumed that the radius of curvature of the actuator patch is $(R + h/2 + h^a/2) \approx R$, where h is the stator thickness and h^a is the actuator thickness. Thus, the effective actuator area S^e can be approximated as $Rb(\phi_2 - \phi_1)$.

It is assumed that only a transverse voltage ϕ^a is applied. If the electrode resistance is neglected, the voltage across the piezoelectric actuator patch is constant. Thus, an actuator voltage $\phi^a(y, \phi, t)$ applied to the distributed piezoelectric actuator patch is

$$\phi^a(y, \phi, t) = \phi^a(t)[u_s(y - y_1) - u_s(y - y_2)][u_s(\phi - \phi_1) - u_s(\phi - \phi_2)], \tag{26}$$

where u_s represents a unit step function, $u_s(\phi - \phi_i) = 1$, when $\phi \geqslant \phi_i$, and $u_s(\phi - \phi_i) = 0$ when $\phi < \phi_i$. The spatial derivative becomes

$$\frac{\partial}{\partial\phi}\phi^a(y, \phi, t) = \phi^a(t)[u_s(y - y_1) - u_s(y - y_2)][\delta(\phi - \phi_1) - \delta(\phi - \phi_2)]. \tag{27}$$

where $\delta(\cdot)$ is the Dirac delta function: $\delta(\phi - \phi_i) = 1$ when $\phi = \phi_i$, and $= 0$ when $\phi \neq \phi_i$. Then, a membrane control force $N_{\phi\phi}^c$ and a control moment $M_{\phi\phi}^c$ in the ϕ-direction induced by the piezoelectric actuator patch can be defined as

$$N_{\phi\phi}^c = Y_p d_{31}\phi^a[u_s(y - y_1) - u_s(y - y_2)][u_s(\phi - \phi_1) - u_s(\phi - \phi_2)], \tag{28}$$

$$M_{\phi\phi}^c = r^a Y_p d_{31}\phi^a[u_s(y - y_1) - u_s(y - y_2)][u_s(\phi - \phi_1) - u_s(\phi - \phi_2)], \tag{29}$$

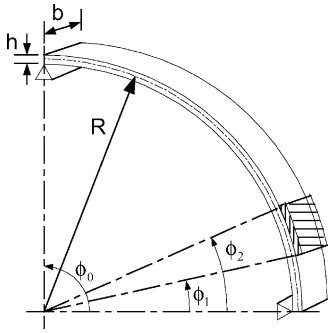

Fig. 3. A piezoelectric laminated circular arc.

where Y_p is the actuator elastic modulus; d_{31} is the piezoelectric strain constant; r^a is the effective moment arm (distance from the neutral surface to the mid-plane of the actuator patch).

3.2. Micro-control actions of curvilinear actuator patches

Actuator control force induced by a segmented patch defined from ϕ_1 to ϕ_2 in the ϕ-direction and from y_1 to y_2 in the y-direction is evaluated and its microscopic membrane/bending characteristics are analyzed. Expanding the modal control force (23) yields

$$\hat{F}_k = \frac{1}{\rho h N_k} \int_y \int_\phi \{L_\phi^c(\phi_3) U_{\phi k} + L_3^c(\phi_3) U_{3k}\} A_1 A_2 \, \mathrm{d}\phi \, \mathrm{d}y. \tag{30}$$

Substituting Love's operators (24) and (25) into the modal force gives

$$\hat{F}_k = \frac{1}{\rho h N_k} \int_y \int_\phi \left\{ \left(-\frac{1}{R} \left(\frac{\partial N_{\phi\phi}^c}{\partial \phi} + \frac{1}{R} \frac{\partial M_{\phi\phi}^c}{\partial \phi} \right) \right) U_{\phi k} + \left(-\frac{1}{R} \left(\frac{1}{R} \frac{\partial^2 M_{\phi\phi}^c}{\partial \phi^2} - N_{\phi\phi}^c \right) \right) U_{3k} \right\} A_1 A_2 \, \mathrm{d}\phi \, \mathrm{d}y. \tag{31}$$

Eq. (31) implies that the modal control force consists of four control force/moment actions. There are (1) the membrane component (or action) $\hat{T}_{k\_\mathrm{mem}\, U\phi}$ induced by $U_{\phi k}$, (2) the bending component $\hat{T}_{k\_\mathrm{bend}\, U\phi}$ induced by $U_{\phi k}$, (3) the membrane component $\hat{T}_{k\_\mathrm{mem} U_3}$ induced by U_{3k}, and (4) the bending component $\hat{T}_{k\_\mathrm{bend}\, U_3}$ induced by U_{3k}. Detailed derivations of control force components are, respectively, defined next.

3.2.1. Membrane control actions

The membrane control force component $\hat{T}_{k\_\mathrm{mem} U\phi}$ induced by $U_{\phi k}$ can be described as

$$\hat{T}_{k\_\mathrm{mem}\, U\phi} = \frac{1}{\rho h N_k} \int_y \int_\phi \left\{ \left(-\frac{1}{R} \frac{\partial N_{\phi\phi}^c}{\partial \phi} \right) U_{\phi k} \right\} A_1 A_2 \, \mathrm{d}\phi \, \mathrm{d}y. \tag{32}$$

Substituting Eqs. (26)–(28) into Eq. (32) gives

$$\hat{T}_{k\_\mathrm{mem}\, U\phi} = \frac{Y_p d_{31} \phi^a}{\rho h N_k} (y_2 - y_1)(U_{\phi k}\big|_{\phi=\phi_2} - U_{\phi k}\big|_{\phi=\phi_1}). \tag{33}$$

Assume the piezoelectric actuator patch has the same width as the arc stator, i.e., $y_2 - y_1 = b$ and also define $U_{\phi k}|_{\phi=\phi_i} = U_{\phi_i k}$. The membrane control force component induced by $U_{\phi k}$ of an actuator patch $[\phi_1 \ \phi_2]$ can be rewritten as

$$\hat{T}_{k\_\mathrm{mem}\, U\phi} = \frac{Y_p d_{31} \phi^a b}{\rho h N_k} (U_{\phi_2 k} - U_{\phi_1 k}). \tag{34}$$

Following the same procedures, one can write the membrane control force component $\hat{T}_{k\_\mathrm{mem}\, U_3}$ induced by U_{3k} as

$$\hat{T}_{k\_\mathrm{mem}\, U_3} = \frac{1}{\rho h N_k} \int_y \int_\phi \left\{ \frac{1}{R} N_{\phi\phi}^c U_{3k} \right\} A_1 A_2 \, \mathrm{d}\phi \, \mathrm{d}y, \tag{35a}$$

$$\hat{T}_{k\_\mathrm{mem}U_3} = \frac{Y_p d_{31}\phi^a}{\rho h N_k}(y_2 - y_1)\int_{\phi_1}^{\phi_2} U_{3k}\,\mathrm{d}\phi. \tag{35b}$$

Thus, the membrane control component induced by U_{3k} of an actuator patch $[\phi_1\ \phi_2]$ becomes

$$\hat{T}_{k\_\mathrm{mem}U_3} = \frac{Y_p d_{31}\phi^a b}{\rho h N_k}\int_{\phi_1}^{\phi_2} U_{3k}\,\mathrm{d}\phi. \tag{36}$$

3.2.2. Bending control actions

The bending control component $\hat{T}_{k\_\mathrm{bend}\,U\phi}$ induced by $U_{\phi k}$ can be described as

$$\hat{T}_{k\_\mathrm{bend}U\phi} = \frac{1}{\rho h N_k}\int_y\int_\phi \left\{\left(-\frac{1}{R^2}\frac{\partial M^c_{\phi\phi}}{\partial\phi}\right)U_{\phi k}\right\}A_1A_2\,\mathrm{d}\phi\,\mathrm{d}y. \tag{37a}$$

Substituting Eqs. (26), (27) and (29) into Eq. (37a) yields

$$\hat{T}_{k\_\mathrm{bend}U\phi} = \frac{r^a Y_p d_{31}\phi^a}{R\rho h N_k}(y_2 - y_1)(U_{\phi k}|_{\phi=\phi_2} - U_{\phi k}|_{\phi=\phi_1}). \tag{37b}$$

Thus, the bending control component induced by $U_{\phi k}$ can be expressed as

$$\hat{T}_{k\_\mathrm{bend}U\phi} = \frac{r^a Y_p d_{31}\phi^a b}{R\rho h N_k}(U_{\phi_2 k} - U_{\phi_1 k}). \tag{38}$$

Furthermore, one can follow the same procedures and define the bending control component $\hat{T}_{k\_\mathrm{bend}U_3}$ induced by U_{3k} as

$$\hat{T}_{k\_\mathrm{bend}U_3} = \frac{1}{\rho h N_k}\int_y\int_\phi \left\{-\frac{1}{R^2}\frac{\partial^2 M^c_{\phi\phi}}{\partial\phi^2}U_{3k}\right\}A_1A_2\,\mathrm{d}\phi\,\mathrm{d}y, \tag{39a}$$

$$\hat{T}_{k\_\mathrm{bend}U_3} = \frac{r^a Y_p d_{31}\phi^a}{R\rho h N_k}(y_2 - y_1)\left(\left.\frac{\partial U_{3k}}{\partial\phi}\right|_{\phi=\phi_1} - \left.\frac{\partial U_{3k}}{\partial\phi}\right|_{\phi=\phi_2}\right). \tag{39b}$$

Consequently, the bending control component induced by U_{3k} can be expressed as

$$\hat{T}_{k\_\mathrm{bend}U_3} = \frac{r^a Y_p d_{31}\phi^a b}{R\rho h N_k}\left(\left.\frac{\partial U_{3k}}{\partial\phi}\right|_{\phi=\phi_1} - \left.\frac{\partial U_{3k}}{\partial\phi}\right|_{\phi=\phi_2}\right). \tag{40}$$

Accordingly, actuator characteristics and all microscopic membrane and bending control actions in the modal force, (31) can be expressed as

$$\hat{F}_k = \hat{T}_{k\_\mathrm{mem}U\phi} + \hat{T}_{k\_\mathrm{mem}U_3} + \hat{T}_{k\_\mathrm{bend}U\phi} + \hat{T}_{k\_\mathrm{bend}U_3}. \tag{41}$$

The modal control force $\hat{F}_k$ and its membrane/bending components $\hat{T}_{k\_iUj}$ depend on actuator locations, modal characteristics, actuator material properties and control voltage. To calculate the actual modal control force and membrane/bending components, the material properties need to be evaluated and a *modal actuation factor* $(\hat{F}_k/\phi^a)$ is defined as the magnitude of the modal force per unit control voltage [(N/kg)/V]. Detailed membrane and bending actuation factors are evaluated in case studies presented next.

4. Parametric study of curvilinear arc stator

A simply supported circular arc stator bonded with a piezoelectric actuator patch laminated from ϕ_1 to ϕ_2 was defined previously in Fig. 3. Vibration characteristics and micro-control actions of the curvilinear arc stator is presented in this section. Standard dimensions of the circular arc are arc radius $R = 60\,\text{mm}$, arc width $b = 9\,\text{mm}$, arc thickness $h = 1\,\text{mm}$, arc angle $\phi_0 = \pi/2$, and piezoelectric lead zirconate titanate (PZT-4) actuator thickness $h^a = 0.5\,\text{mm}$. Material properties of the circular arc stator and piezoelectric actuator are summarized in Table 1.

First, vibration characteristics and odd/even flexural mode shapes of the arc stator are studied to determine suitable position and size of the actuator patch. Then, parametric analysis of design parameters, such as arc thickness, actuator thickness and arc radius, is conducted to evaluate actuator characteristics and micro- membrane/bending control actions.

4.1. Vibration characteristics and design of the curvilinear arc stator

The analytical solutions, as previously discussed in Eqs. (13) and (14) and (16) and (17), imply that transverse flexural mode shapes in the radial direction dominates at the higher natural modes. Note that the modal analysis (i.e., natural frequencies and mode shapes) of the curvilinear arc stator is based on the original elastic stator, so that external excitations (both mechanical and electrical) are excluded. (Hence, the control force $N^c_{\phi\phi}$ and moment $M^c_{\phi\phi}$ resulting from the electrical excitation ϕ^a are neglected in the modal analysis.) With the material and geometry defined for the curvilinear arc stator, one can further examine the flexible modes U_{3k} of the arc stator ($\phi_0 = \pi/2$) and plot modes $k = 2$–9 in Fig. 4. In order to avoid audible noise during operation, the curvilinear arc stator is designed to operate at ultrasonic frequency range (above 20 kHz). Hence, the 9th mode at 21,113 Hz is chosen as the driving frequency. Furthermore, based on the 9th flexible mode shape and nodal lines, a segmented actuator patch ($\pi/18$) is placed on the circular arc from $\phi_1 = \pi/18$ to $\phi_2 = 2\pi/18$ based on the nodal lines and wavelength of the 9th flexural mode. Micro-control actions and control characteristics of the actuator patch ($\phi_1 = \pi/18$ and $\phi_2 = 2\pi/18$) are evaluated next.

Table 1
Material properties

	Lead zirconate titanate PZT-4 actuator [20]	Steel circular arc	Unit
Young's modulus	$Y_p = 80$	$Y = 210$	GPa
Density	$\rho_p = 7550$	$\rho = 7860$	kg/m^3
Poisson's ratio	$\mu_p = 0.34$	$\mu = 0.27$	
Piezoelectric constant			
d_{31}	-1.2×10^{-10}		m/V
e_{33}	15.1		C/m^2
e_{31}	-5.2		C/m^2
e_{15}	12.7		C/m^2
Permittivity (ε_{33})	1.15×10^{-8}		F/m

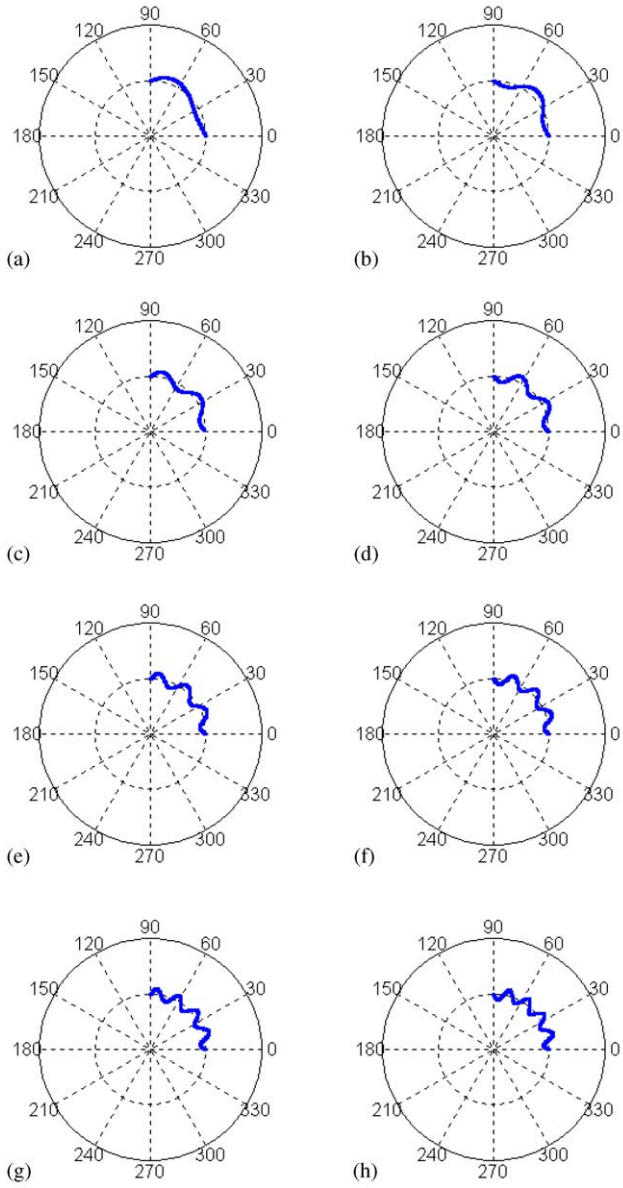

Fig. 4. Flexural mode shapes U_{3k} of the circular arc ($\phi_0 = \pi/2$): (a) $k = 2$; (b) $k = 3$; (c) $k = 4$; (d) $k = 5$; (e) $k = 6$; (f) $k = 7$; (g) $k = 8$; (h) $k = 9$ modes.

4.2. Micro-control actions of the curvilinear arc stator

In this section, the modal control force is investigated in terms of the *modal actuation factor* defined previously. Parametric analysis of design parameters, i.e., arc radius, arc thickness and actuator thickness, is carried out to evaluate actuation characteristics of the designed piezoelectric

actuator (i.e., a $\pi/18$ patch placed at $\phi_1 = \pi/18$ and $\phi_2 = 2\pi/18$). Numerical data of modal actuation factor and contributing components, i.e., $\hat{T}_{k\_\text{mem}U\phi}$, $\hat{T}_{k\_\text{mem}U_3}$, $\hat{T}_{k\_\text{bend}U\phi}$ and $\hat{T}_{k\_\text{bend}U_3}$, are investigated with respect to various design parameters and compared with the standard dimension.

4.2.1. Case 1: arc thickness

The circular arc thickness is varied from 1 to 5 mm. The total modal actuation factor ($\hat{F}_k/\phi^a$) and its membrane and bending components of the first 12 modes are plotted in Figs. 5 and 6, respectively.

Fig. 5 shows that the 9th modal actuation factor indeed has the maximal contribution compared with the others. It confirms that the actuator location is well selected to excite the arc stator at the 9th natural mode. Furthermore, at this actuator location, the 6th and 12th modal actuation factors are zero implying that the actuator does not excite those modes at all. Furthermore, modal actuation factors and their detailed micro-membrane and bending control action components are plotted in Fig. 6.

The magnitude of modal membrane component $\hat{T}_{k\_\text{mem}U\phi}$ induced by U_ϕ is very close to that of the modal membrane component $\hat{T}_{k\_\text{mem}U_3}$ induced by U_3 but with an opposite sign. This causes the sum of the membrane actuation factor to be approximately zero. The magnitude of the modal bending component $\hat{T}_{k\_\text{bend}U\phi}$ induced by U_ϕ is very small. This can be explained by comparing Eq. (34) with Eq. (38), and it shows that $\hat{T}_{k\_\text{bend}U\phi}$ equals to $(r^a/R) \times \hat{T}_{k\_\text{mem}U\phi}$ and r^a/R is very small. The modal bending component $\hat{T}_{k\_\text{bend}U_3}$ induced by U_3 dominates the overall modal actuation factor since summation of other three components ($\hat{T}_{k\_\text{mem}U\phi} + \hat{T}_{k\_\text{mem}U_3} + \hat{T}_{k\_\text{bend}U\phi}$) is very small. For a thin arc stator at lower natural modes, the magnitude of the membrane component is larger than that of the bending component (e.g., Fig. 6 at $k = 2$ and 3). At higher

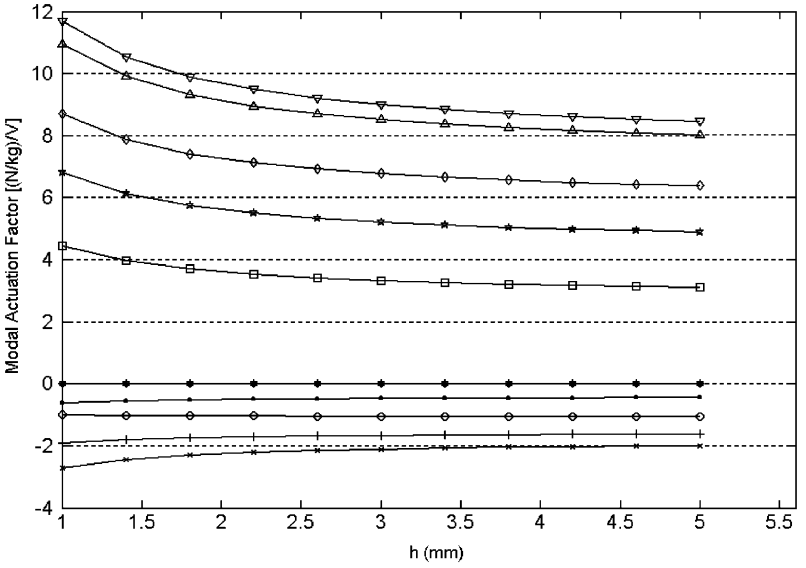

Fig. 5. Modal actuation factor of various arc thickness: ■, $k = 2$; ◇, $k = 3$; ×, $k = 4$; +, $k = 5$; ∗, $k = 6$; □, $k = 7$; ◇, $k = 8$; ▽, $k = 9$; △, $k = 10$; ⋆, $k = 11$, ✡, $k = 12$ modes.

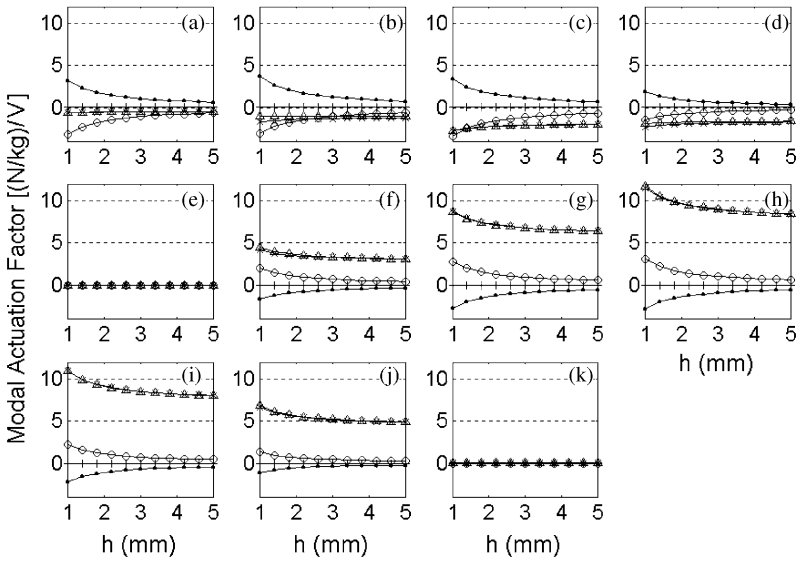

Fig. 6. Modal actuation factor components of various arc thickness: (a) $k = 2$; (b) $k = 3$; (c) $k = 4$; (d) $k = 5$; (e) $k = 6$; (f) $k = 7$; (g) $k = 8$; (h) $k = 9$; (i) $k = 10$; (j) $k = 11$; (k) $k = 12$ modes. ■, $\hat{T}_{k\_\mathrm{mem}U\phi}$; ◇, $\hat{T}_{k\_\mathrm{mem}U_3}$; +, $\hat{T}_{k\_\mathrm{bend}U\phi}$; ×, $\hat{T}_{k\_\mathrm{bend}U_3}$; △, $\hat{F}_k$.

natural modes where the modal actuation factors are not zero, the magnitude of the bending components dominates the overall actuation behavior, and thus generates a curvilinear driving action.

The modal actuation factors decrease and approach constant as the arc thickness increases because the increased shell rigidity affecting all membrane and bending components. That is, (1) the magnitudes of the membrane components $\hat{T}_{k\_\mathrm{mem}U\phi}$ and $\hat{T}_{k\_\mathrm{mem}U_3}$ decrease due to the increased shell rigidity as it also reflects in the equations of membrane components (Eqs. (34) and (36)) that they are inversely proportional to the arc thickness; (2) the magnitudes of the bending components $\hat{T}_{k\_\mathrm{bend}U\phi}$ and $\hat{T}_{k\_\mathrm{bend}U_3}$ decrease and approach constant. It is obviously noticeable that when substituting $r^a = h/2 + h^a/2$ into the bending component equations (e.g., Eqs. (38) and (40)) they become a summation of an arc-thickness independent term and a term proportional to h^a/h. The (h^a/h) becomes insignificant as the arc thickness increases. Thus, the bending components decrease and approach constants as the arc thickness increases.

4.2.2. Case 2: actuator thickness

In this case, the PZT actuator thickness changes from 0.5 to 1 mm. The modal actuation factor and its membrane and bending control components of the first 12 modes are, respectively, plotted in Figs. 7 and 8.

The magnitudes of non-zero modal actuation factors increase linearly as the actuator thickness increases as shown in Fig. 7, due to the increased modal bending components. Examining the modal micro-actuation components illustrated in Fig. 8, it shows that the magnitudes of $\hat{T}_{k\_\mathrm{mem}U\phi}$

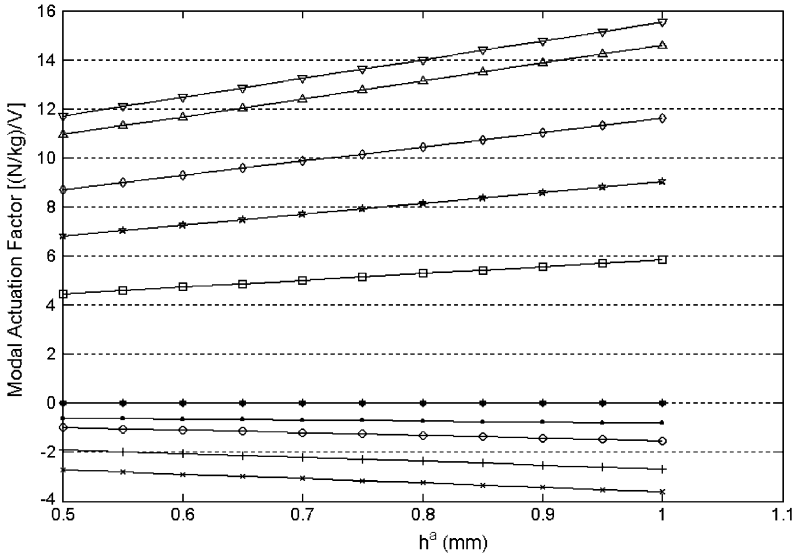

Fig. 7. Modal actuation factor of various actuator thickness: ■, $k = 2$; ◇, $k = 3$; ×, $k = 4$; +, $k = 5$; ∗, $k = 6$; □, $k = 7$; ◇, $k = 8$; ▽, $k = 9$; △, $k = 10$; ⋆, $k = 11$; ✡, $k = 12$.

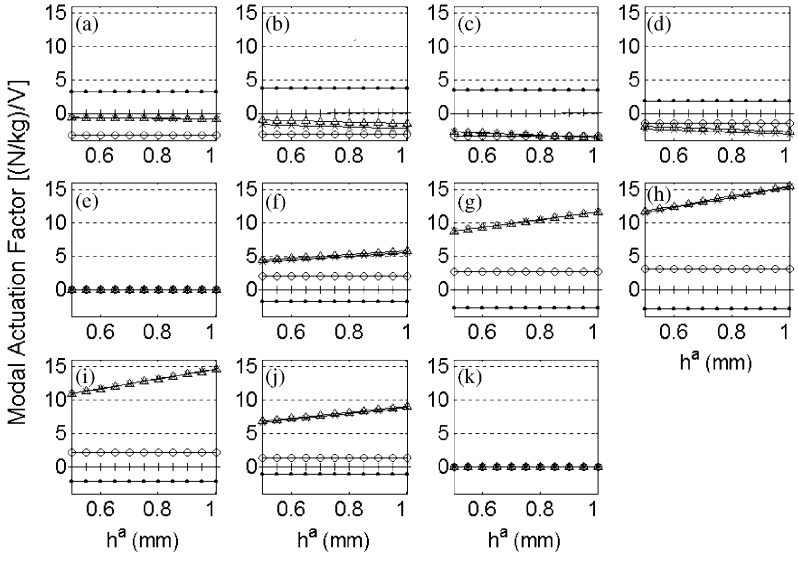

Fig. 8. Modal actuation factor components of various actuator thickness: (a) $k = 2$; (b) $k = 3$; (c) $k = 4$; (d) $k = 5$; (e) $k = 6$; (f) $k = 7$; (g) $k = 8$; (h) $k = 9$; (i) $k = 10$; (j) $k = 11$; (k) $k = 12$ modes. ■, $\hat{T}_{k\_\mathrm{mem}U\phi}$; ◇, $\hat{T}_{k\_\mathrm{mem}U_3}$; +, $\hat{T}_{k\_\mathrm{bend}U\phi}$; ×, $\hat{T}_{k\_\mathrm{bend}U_3}$; △, $\hat{F}_k$.

and $\hat{T}_{k\_\mathrm{mem}U_3}$ are constant since they are actuator-thickness independent and $\hat{T}_{k\_\mathrm{bend}U_3}$ increases linearly as the actuator thickness increases and it dominates the overall modal actuation factor because summation of other three components is very small as discussed previously.

4.2.3. Case 3: arc radius

In this case, the circular arc radius changes from 60 to 80 mm. The modal actuation factor and its detailed membrane and bending components of the first 12 modes are plotted in Figs. 9 and 10.

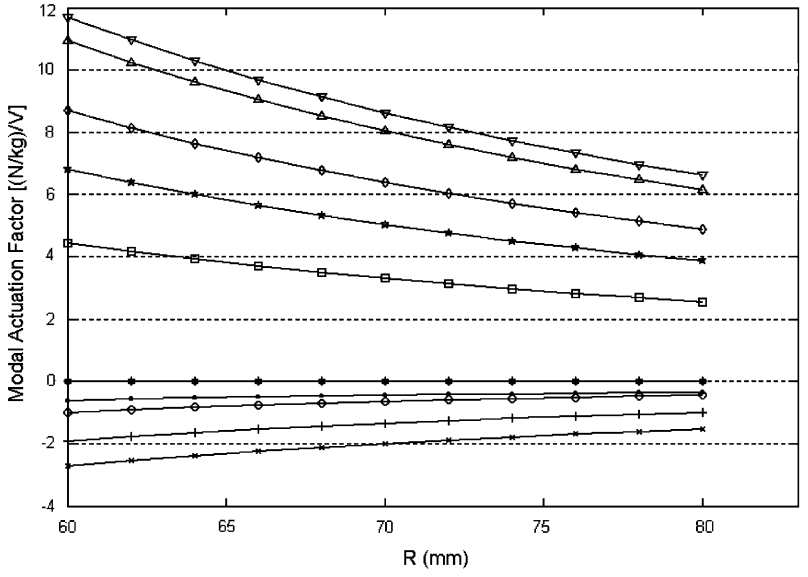

Fig. 9. Modal actuation factor of various arc radius: ■, $k = 2$; ◇, $k = 3$; ×, $k = 4$; +, $k = 5$; ∗, $k = 6$; □, $k = 7$; ◇, $k = 8$; ▽, $k = 9$; △, $k = 10$; ⋆, $k = 11$; ☆, $k = 12$ modes.

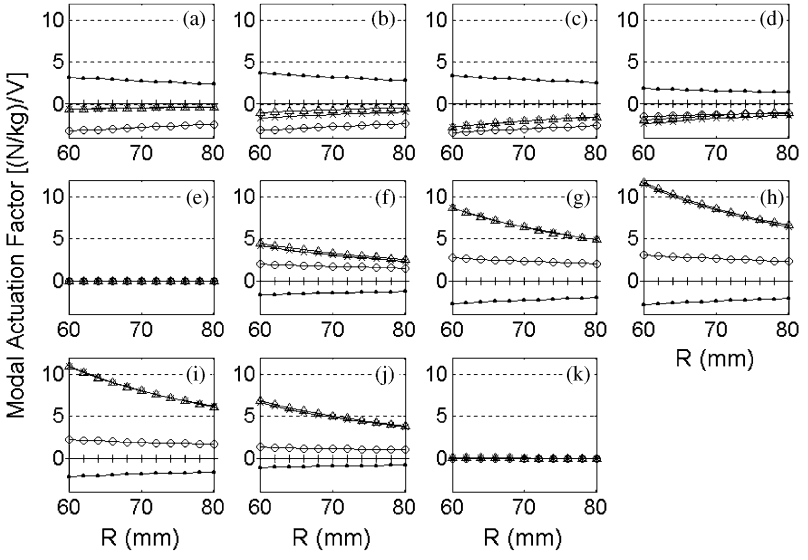

Fig. 10. Modal actuation factor component of various arc radius: (a) $k = 2$; (b) $k = 3$; (c) $k = 4$; (d) $k = 5$; (e) $k = 6$; (f) $k = 7$; (g) $k = 8$; (h) $k = 9$; (i) $k = 10$; (j) $k = 11$; (k) $k = 12$ modes. ■, $\hat{T}_{k\_\mathrm{mem}U\phi}$; ◇, $\hat{T}_{k\_\mathrm{mem}U_3}$; +, $\hat{T}_{k\_\mathrm{bend}U\phi}$; ×, $\hat{T}_{k\_\mathrm{bend}U_3}$; △, $\hat{F}_k$.

Fig. 9 shows that the modal actuation factor decreases as the arc radius increases. Examining Eqs. (34), (36) (38) and (40) implies that (1) the magnitudes of the membrane components are inversely proportional to the arc radius since N_k is proportional to the arc radius and (2) the magnitudes of the bending components are proportional to $1/R^2$, hence they decrease faster than the membrane components as the arc radius increases, Fig. 10. For these reasons, the modal actuation factor decreases as the arc radius increases.

5. Conclusions

Ultrasonic vibration behavior has long been utilized in ultrasonic motors and drivers. This study is to evaluate ultrasonic vibration characteristics and micro-control actions of a curvilinear arc stator bonded with a piezoelectric PZT actuator patch. Mathematical models of the arc stator and its membrane and bending control characteristics were formulated first. Modal actuation factors, including in-plane and transverse membrane/bending micro-control actions, were analyzed with respect to key design parameters, e.g., arc thickness, actuator thickness and arc radius. Study of stator vibration behavior clearly suggests an optimal actuator size and location to efficiently excite the desirable ultrasonic natural mode. Based on designed actuator size and location, the bending actuation component induced by the transverse U_3 dominates the overall modal control force for high natural modes and efficiently excites the desirable ultrasonic natural mode. Parametric study of design parameters reveals that (1) the magnitudes of modal actuation factors decrease and approach constants as the arc thickness increases, (2) the magnitudes of modal actuation factors increase linearly as the actuator thickness increases, due to the increased modal bending components, and (3) the magnitudes of modal actuation factors decrease as the arc radius increases.

Accordingly, based on the methodology and parametric evaluation presented in this study, one can design an optimal PZT actuator (size) placed at a specific location on the arc stator to effectively generate flexible (bending) vibration at a specified ultrasonic natural frequency. To achieve higher modal control force at ultrasonic operating frequency, the actuator pattern (i.e., size and location) and operating frequency should be designed based on the natural mode shape and frequency while the arc stator radius should remain small. Also, the bending control action can be enhanced by reducing arc thickness and/or increasing the actuator thickness. The micro-bending control action dominates at high natural modes and it becomes a driving wave when appropriate input amplitude and phase are selected for the curvilinear arc stator. (This wave driving behavior of the curvilinear arc stator will be reported separately.)

References

[1] T. Sashida, T. Kenjo, *An Introduction to Ultrasonic Motors*, Clarendon Press, Oxford, 1993.
[2] S. Ueha, Y. Tomikawa, M. Kurosawa, N. Nakamura, *Ultrasonic Motors: Theory and Applications*, Clarendon Press, Oxford, 1993.
[3] K. Uchino, Piezoelectric ultrasonic motors: overview, *Smart Material and Structures* 7 (1998) 273–285.

[4] H.S. Tzou, *Piezoelectric Shells (Distributed Sensing and Control of Continua)*, Kluwer Academic Publishers, Boston, 1993.
[5] H.S. Tzou, H.Q. Fu, A study of segmentation of distributed piezoelectric sensors and actuators, Part II: parametric study and active vibration controls, *Journal of Sound and Vibration* 172 (2) (1994) 261–275.
[6] S.H. Chen, Z.D. Wang, X.H. Liu, Active vibration control and suppression for intelligent structures, *Journal of Sound and Vibration* 200 (2) (1997) 167–177.
[7] H.S. Tzou, P. Smithmaitrie, J.H. Ding, Micro-sensor electromechanics and distributed signal analysis of piezo(electric)-elastic spherical shells, *Mechanical Systems and Signal Processing* 16 (2–3) (2002) 185–199.
[8] H. S Tzou, Y. Bao, V.B. Venkayya, Microelectromechanics and functionality of segmented cylindrical transducers, in: A. Guran, H.S. Tzou (Eds.), *Structronic Systems: Structure Devices & Systems, Part I*, World Scientific Publishing, Singapore, 1998, pp. 151–196.
[9] H.S. Tzou, D.W. Wang, W.K. Chai, Dynamics and distributed control of conical shells laminated with full and diagonal actuators, *Journal of Sound and Vibration* 256 (1) (2002) 65–79.
[10] H.S. Tzou, J.H. Ding, I. Hagiwara, Micro-control actions of segmented actuator patches laminated on deep paraboloidal shells, *JSME International Journal C* 45 (1) (2002) 8–15.
[11] P. Smithmaitrie, H.S. Tzou, Micro-control actions of actuator patches laminated on hemispherical shells, *Proceedings of IMECE2002 ASME International Mechanical Engineering Congress & Exposition*, New Orleans, LA, 2002 CD-ROM IMECE2002-33570.
[12] H.T. Banks, Y. Zhang, Computational method for a curved beam with piezoceramic patches, *Journal of Intelligent Material System and Structures* 8 (3) (1997) 260–278.
[13] V.R. Sonti, J.D. Jones, Curved piezoactuator model for active vibration control of cylindrical shells, *AIAA Journal* 34 (5) (1996) 1034–1040.
[14] J.H. Qiu, J.J. Tani, Vibration control of a cylindrical-shell distributed piezoelectric sensors and actuators, *Journal of Intelligent Material System and Structures* 6 (4) (1995) 474–481.
[15] H.R. Shih, Distributed vibration sensing and control of a piezoelectric laminated curved beam, *Smart Materials and Structures* 9 (6) (2000) 761–766.
[16] P. Smithmaitrie, J.G. DeHaven, K. Higuchi, H.S. Tzou, Harmonic wave propagation of ultrasonic arc stators, *Proceedings of IMECE2003 ASME International Mechanical Engineering Congress & Exposition*, Washington, DC, 2003 CD-ROM IMECE2003-42417.
[17] R.D. Blevins, *Formulas for Natural Frequency and Mode Shape*, reprint ed., Krieger, Melbourne, FL, 1995.
[18] A.S. Veletsos, W.J. Austin, C.A. Lopes Pereira, S.J. Wung, Free in-plane vibration of circular arches, *Journal of the Engineering Mechanics Division* 98 (1972) 311–329.
[19] W. Soedel, *Vibrations of Shells and Plates*, Marcel Dekker, New York, 1981.
[20] O.E. Mattiat, *Ultrasonic Transducer Materials*, Plenum Press, New York, 1971.